# Origin of Stereoselectivity of the Alkylation of Cyclohexadienone-Derived Bicyclic Malonates

Kelly A. Volp and Andrew M. Harned*

Department of Chemistry, University of Minnesota—Twin Cities, 207 Pleasant St. SE, Minneapolis, Minnesota 55455, United States

Ⓢ *Supporting Information*

ABSTRACT: The diastereoselectivity of the alkylation of bicyclic malonates has been studied experimentally and computationally. In accordance with previous observations during a total synthesis of sorbicillactone A, alkylations involving methyl iodide proceed from the concave (endo) face of the bicyclo[4.3.0]nonene ring system. In contrast,

carbon-based electrophiles larger than methyl iodide approach from the convex (exo) face. Computational studies using M06-2X and B3LYP methods have revealed that the observed stereoselectivity is explained by subtle energetic differences between a staggered transition state with less torsional strain and unfavorable steric interactions with the cyclohexenone ring. Using this model as a guide, hydrogenation of the C−C double bond was used to alter the steric environment of the substrate. As expected, this led to a reversal in the diastereoselectivity during the alkylation with methyl iodide.
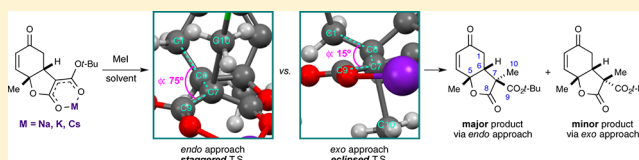
1. INTRODUCTION

The biological activity of a particular compound is intimately related to its three-dimensional structure. With this in mind, synthetic chemists often agonize over controlling the configuration (both relative and absolute) of newly formed stereogenic carbon atoms. Consequently, the development of predictive models for the stereoselective construction of C−C bonds is of central importance for complex molecule synthesis.[1,2] Some of the more reliable strategies for stereoselective synthesis involve using existing stereochemical elements to direct the formation of new stereocenters.[3] Several such approaches have been developed that have proven to be quite general.[4−6] The discovery of examples that run counter to established models provides an opportunity to further refine these models and deepen our understanding of stereoselective processes in general.

The sorbicillactones are members of the sorbicillinoid family of natural products[7] that were first isolated by Bringmann and co-workers in the early 2000s.[8,9] Initial biological testing revealed that sorbicillactone A has anticancer, anti-HIV, and possible neuroprotective activity. Conversely, sorbicillactone B did not have any reported biological activity.[9] We were intrigued by this biological profile and sought to develop a synthetic route to the sorbicillinoid framework that would be amenable to the production of other analogues for further biological evaluation. Although synthetic routes to other members of the sorbicillinoid family have been reported,[7] the incorporation of the amino acid alanine into the sorbicillactone structure introduces synthetic challenges that are unique to the sorbicillactones.

We sought to construct the bicyclic core of the sorbicillactones using a tandem conjugate addition/alkylation of malonate-tethered cyclohexadienone 1 (Scheme 1). It was anticipated that the cis-fused bicyclic nature of the intermediate

Sorbicillactone A

Sorbicillactone B
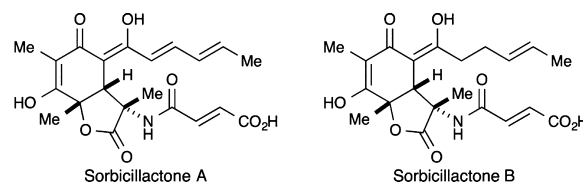
malonate anion 2 would cause the alkylating agent (MeI) to approach from the convex (exo) face and form the C7 stereocenter with the correct configuration. In practice, the initial cyclization of 1 did prove to be an excellent means to establish the correct relative configuration at C5 and C6. However, we were surprised to find that the alkylation event formed ***endo*-3**,[10] containing an α-Me group at C7, as the major diastereomer. Nevertheless, performing this cyclization/alkylation reaction on a multigram scale allowed us to isolate over 1 g of the desired diastereomer (***exo*-3**), a sufficient quantity to complete the total synthesis of sorbicillactone A.[11]

The stereoselectivity displayed by this reaction sequence was quite surprising considering that formation of the major diastereomer (***endo*-3**) requires the electrophile to approach bicyclic malonate anion 2 from the seemingly more crowded endo (concave) face. This is counter to what is commonly perceived as a reliable strategy for stereoinduction.[12] Indeed, a search of the literature revealed that alkylations of similar bicyclic lactones typically do proceed from the exo (convex) face.[13−15] With these results in mind, we set out to identify both the generality and the origin of this surprising stereoselectivity. Herein, we report a combined experimental and theoretical study aimed at answering the following questions: (1) What is the source of this unexpected stereochemical
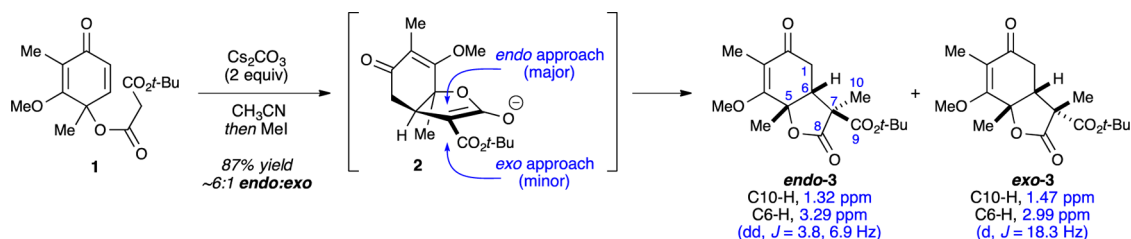
Scheme 1

Table 1. Influence of Solvent on Diastereoselectivity

entry[a]	solvent	dielectric constant[b]	time (h)	% conversion[c]	dr (endo:exo)[c]	% yield[d]
1	CH$_3$CN	36.64	2	79	5.3:1	65
2	CH$_3$CN	36.64	6	100	5.5:1	93
3	DMF	38.25	18	100	5.8:1	95
4	acetone	21.01	5.5	100	3.7:1	89
5	CH$_2$Cl$_2$	8.93	24	71	3.6:1	60
6	DME	7.30	12	100	1.6:1	93
7	THF	7.52	2	58	1.5:1	51
8	THF	7.52	6	84	1.5:1	76
9	THF	7.52	14	100	1.5:1	91
10	dioxane	2.22	18	84	1.3:1	66
11[e]	MTBE	~4[f]	48	96	1.7:1	71

[a]All reactions performed at rt using 0.131 mmol of **6**, 1.2 equiv of Cs$_2$CO$_3$, and 1.2 equiv of MeI in the listed solvent (0.08 M). [b]Values obtained from ref 17. [c]Measured by HPLC. [d]Combined yield calculated by quantitative NMR (qNMR), Ph$_3$CH as an internal standard. [e]After 24 h at rt, the temperature was raised to 60 °C and stirred for another 24 h. [f]The dielectric constant of MTBE has not been reported. The estimated value is based on the dielectric constant of diethyl ether (4.27) and diisopropyl ether (3.81).

outcome? (2) Can alternative substrates be devised that lead to a stereochemical outcome that is more useful for our purposes?

2. RESULTS AND DISCUSSION

2.1. Experimental Results. *2.1.1. Model System: Influence of Reaction Conditions.* To gain more insight into the influence of reaction conditions on the stereoselectivity of this process, we decided to employ a more readily accessible model system. Thus, the one-pot cyclization/alkylation of *p*-cresol-derived dienone **4** was performed using our previously reported conditions[11] (Scheme 2). The reaction proceeded with the same level of diastereoselectivity as the original system (i.e., **1** → **3**). The identity of ***endo*-5** and ***exo*-5** was established by comparing the chemical shifts of the methyl groups and C6 methyne protons in **5** with those of the analogous protons in **3**, the structure of which was established through X-ray analysis of a derivative.[11]

Having confirmed that the cyclization/alkylation of **4** is indeed a valid model reaction, we decided to evaluate the influence of solvent and base on the diastereoselectivity (Tables 1 and 2, respectively). To facilitate this effort, dienone **4** was cyclized to give bicyclic malonate **6** (Scheme 3), a compound we had previously synthesized during a related methodology study.[16] Importantly, the alkylation of **6** in acetonitrile proceeded to give **5** with the same diastereoselectivity as the one-pot process (Table 1, entries 1 and 2).

The results of the solvent screen are shown in Table 1. Changing the solvent from acetonitrile to another polar solvent (DMF) had a negligible influence on the endo:exo ratio (entry 3). In contrast, using a solvent of either moderate (acetone) or low polarity (CH$_2$Cl$_2$) proceeded with lower endo selectivity (entries 4 and 5). Curiously, all ethereal solvents (entries 6–11) had diminished endo selectivity, irrespective of their

Scheme 2
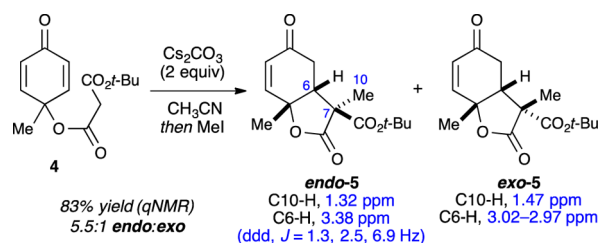
Scheme 3
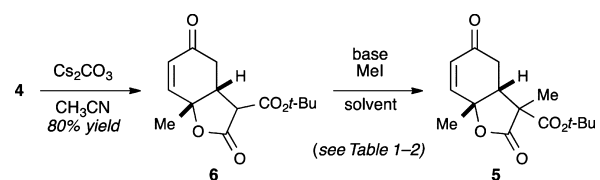
polarity (entries 6, 9–11) or conversion (entries 7–9). Modified reaction conditions were required when methyl *t*-butyl ether (MTBE) was used as solvent (entry 11).

The choice of base had a complex influence on both reaction efficiency and diastereoselectivity (Table 2). Switching from Cs$_2$CO$_3$ to K$_2$CO$_3$ lowered the diastereoselectivity of the alkylation (entries 1 and 2). In contrast, the strong amine base DBU resulted in a somewhat higher diastereoselectivity, albeit with diminished reactivity (entry 6). No reaction was observed with Na$_2$CO$_3$, Li$_2$CO$_3$, or MgO (entries 3–5), likely due to a lack of solubility.

The use of DBU presumably results in a coordination environment that is much different from that formed when inorganic bases are used. To further explore this, the reaction

Table 2. Influence of Base on Diastereoselectivity

entry[a]	base	solvent	time (h)	% conversion[b]	dr (endo:exo)[b]	% yield[c]
1	Cs_2CO_3	CH_3CN	6	100	5.5:1	93
2	K_2CO_3	CH_3CN	16	88	4.6:1	85
3	Na_2CO_3	CH_3CN	16	0		
4	Li_2CO_3	CH_3CN	16	0		
5	MgO	CH_3CN	16	0		
6	DBU	CH_3CN	16	45	6.2:1	43
7[d]	K_2CO_3/18-crown-6	CH_3CN	24	100	6.4:1	88
8[d]	K_2CO_3/18-crown-6	THF	24	94	3.3:1	74
9	Cs_2CO_3	10:1 THF/HMPA	30	100	1.6:1	82
10	Cs_2CO_3	1:1 THF/HMPA	30	92	3.1:1	67
11[e]	NaH	THF	48	100	0.9:1	79

[a]All reactions performed at rt using 0.131 mmol of **6**, 1.2 equiv of the listed base, and 1.2 equiv of MeI in the listed solvent (0.08 M). [b]Measured by HPLC. [c]Combined yield calculated by qNMR, Ph_3CH as an internal standard. [d]1.2 equiv of 18-crown-6 was used. [e]After 24 h at rt, the temperature was raised to 60 °C and stirred for another 24 h.

was performed with K_2CO_3 in the presence of 18-crown-6 in order to make the counterion less coordinating. This increased the diastereoselectivity to levels consistent to those obtained with the amidine base (compare entries 2, 6, 7). On the basis of this success, we then returned to the use of ethereal solvents. Using K_2CO_3 with 18-crown-6 in THF increased the amount of *endo*-**5** produced, relative to Cs_2CO_3 in THF (compare Table 2, entry 8 with Table 1, entry 9). To study the influence of additives with Cs_2CO_3, increasing amounts of HMPA were added. Lower concentrations of HMPA had little impact on the diastereoselectivity (compare Table 1, entry 9, and Table 2, entry 9), but higher concentrations resulted in an increase in the amount of *endo*-**5** produced (entry 10).

The final base examined was NaH in THF. This reaction was sluggish and resulted in no diastereoselectivity (Table 2, entry 11). Another notable observation was that the selectivity at partial and full conversion was the same (Table 1, entries 1, 2, 7−9). This suggests that epimerization through a retro-Michael process is not important.[18]

2.1.2. Influence of Electrophile. Having examined the influence of both solvent and base, we turned our attention to the electrophile (Table 3). Given the high degree of endo selectivity observed with MeI, we were surprised to find that all other carbon-based electrophiles were quite selective toward

formation of the exo diastereomer.[19] Only allyl bromide gave any appreciable amount of the endo isomer (entry 4). Although these results were quite disparate from that obtained with MeI, it was gratifying to see that our original hypothesis of alkylation from the convex (exo) face was not without merit. Rather, it became clear that the use of MeI with these particular nucleophiles was an unusual case that warranted closer attention.

2.1.3. Influence of Nucleophile. Finally, we decided to test other bicyclic malonates as nucleophiles. The results of this study are reported in Table 4. Switching the *t*-butyl ester for a benzyl ester (**10**, entry 3) resulted in a slight increase in the endo:exo ratio. Adding a methyl group to the β-position of the enone (**12**, entry 4) had little influence on the diastereoselectivity. Alkylation of the same substrate in THF resulted in diminished selectivity (entry 5), matching the results observed with the model substrate (entry 2). We were also interested in whether these same solvent effects would result in an increase in the formation of the desired exo isomer using our sorbicillactone substrate. Gratifyingly, the alkylation of **14** proceeded with diminished endo selectivity when Cs_2CO_3 or NaH were used in THF (compare entries 6 and 7 with Scheme 1). Finally, the alkylation of **14** with benzyl bromide afforded *exo*-**15** as the exclusive product (Scheme 4).

2.2. Computational Results. To better understand the origin of the stereoselectivity observed with MeI, we performed molecular modeling of several key structures. Specifically, the structures of the deprotonated malonate, diastereomeric products, and alkylation transition states for the model transformation shown in Scheme 5 were considered. Calculations were performed at both the M06-2X[20] and B3LYP[21] levels using the 6-31G(d)[22] basis set (see the Experimental Section for more details). To simplify the calculations, MeI was replaced with MeCl during the transition-state analysis.[23] In general, the computational results using M06-2X and B3LYP led to somewhat different energy differences. This is likely due to the ability of the former to better handle both noncovalent interactions (to include dispersion binding forces and solvation)[24−29] and transition-state analysis.[30,31] Importantly, both methods led to the same conclusions. Wherever relative energy differences are reported, results from B3LYP are given in parentheses.
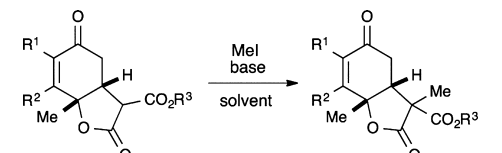
2.2.1. Structure of the Deprotonated Bicyclic Malonate. As stated above, the diastereoselectivity of the alkylation was surprising, given that the major diastereomer seemingly arises

Table 3. Influence of Electrophile on the Diastereoselectivity

entry[a]	electrophile (R−X)	product	dr (endo:exo)[b]	% yield[c]
1	MeI	**5**	5.5:1	93
2	BnBr	**7**	<1:20	92 (89)[d]
3[e]	2-iodopropane	**8**	<1:20	19[d]
4	allyl bromide	**9**	1:6.3	89 (81)[d]

[a]All reactions performed at room temperature using 0.131 mmol of **6**, 1.2 equiv of Cs_2CO_3, and 1.2 equiv of electrophile in acetonitrile (0.08 M) for 16 h. [b]Calculated by ^{1}H NMR of the crude material and confirmed by HPLC. [c]Combined yield calculated from qNMR, Ph_3CH used as an internal standard. [d]Isolated yield after purification by flash column chromatography (SiO_2). [e]Reaction performed at 80 °C for 6 days.

**Table 4. Influence of Nucleophile on Diastereoselectivity**

entry[a]	substrate	product	R[1]	R[2]	R[3]	base	solvent	dr (endo:exo)[b]	% yield[c]
1	6	5	H	H	t-Bu	Cs₂CO₃	CH₃CN	5.5:1	93
2	6	5	H	H	t-Bu	Cs₂CO₃	THF	1.5:1	91
3[d]	10	11	H	H	Bn	Cs₂CO₃	CH₃CN	7.9:1	85
4	12	13	H	Me	t-Bu	Cs₂CO₃	CH₃CN	6.5:1	88
5	12	13	H	Me	t-Bu	Cs₂CO₃	THF	1.5:1	80
6	14	3	Me	OMe	t-Bu	Cs₂CO₃	THF	2.5:1	82
7[e]	14	3	Me	OMe	t-Bu	NaH	THF	1.8:1	40 (60)[f]

[a]All reactions performed at rt using 0.13 mmol of the substrate, 1.2 equiv of base, and 1.2 equiv of MeI in the listed solvent (0.08M) for 16 h. [b]Calculated by achiral HPLC. [c]Combined yield calculated by qNMR, Ph₃CH as an internal standard. [d]Performed using 0.07 mmol of the substrate. [e]After 24 h at rt, the temperature was raised to 60 °C and stirred for another 24 h. [f]Calculated yield based on the presence of 38% starting material.

Scheme 4
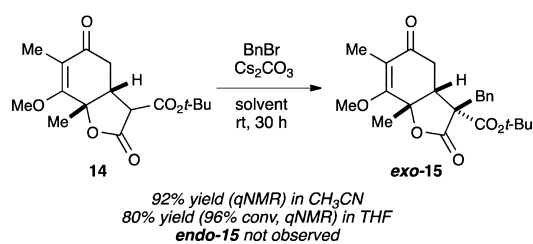
Scheme 5
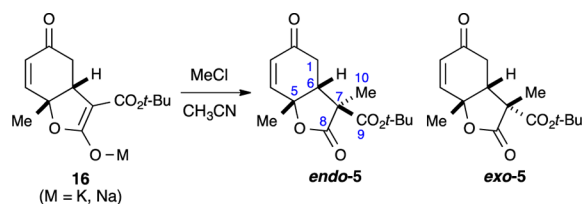
from the more sterically crowded face of the intermediate bicyclic anion. This supposition was evaluated by modeling malonate anion **16** in the presence of either a Na or a K cation.[32] Three potential cation coordination modes were examined (Figure 1a): one syn conformation (**16S**) and two anti conformations (**16A₁** and **16A₂**).[33] With both Na and K, coordination of the metal via syn conformation **16S** was clearly preferred over coordination through either anti conformation. Qualitatively, the concave face (endo approach) of **16S** appeared to be more sterically crowded than the convex face (exo approach) due to the cyclohexenone ring being roughly perpendicular to the plane formed by the metal-coordinated malonate anion (Figure 1b,c). This analysis confirmed that our initial hypothesis with respect to which face is more sterically accessible was not flawed. It also confirms that the observed stereoselectivity is likely due to a confluence of factors, rather than a pure steric influence.

2.2.2. Relative Energy of Alkylated Products. We also considered the possibility that an unidentified equilibration process was responsible for the observed product distribution. This was evaluated by considering the relative energies of the alkylation products **endo-5** and **exo-5** (Figure 2). To account for conformational flexibility with the exocyclic ester, a relaxed scan around the C7−C9 σ-bond was performed (see the
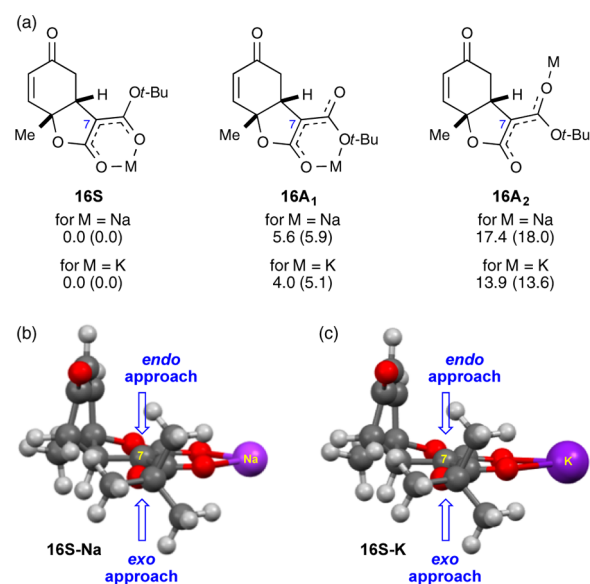

Figure 1. (a) Structure of the sodium and potassium malonates. Values below each structure are relative energies (kcal/mol) calculated by M06-2X (B3LYP). (b) Side view of the calculated (M06-2X) structure of **16S**, M = Na. (c) Side view of the calculated (M06-2X) structure of **16S**, M = K. Front views and structures calculated using B3LYP can be found in the Supporting Information.
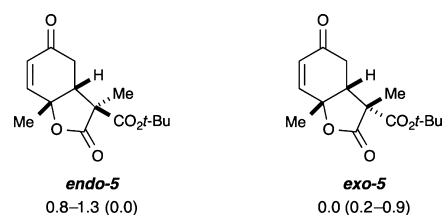

Figure 2. Relative energy (kcal/mol) of the lowest-energy conformers of **endo-5** and **exo-5**. Energies below each structure are calculated by M06-2X (B3LYP). The calculated structures can be found in the Supporting Information.

Experimental Section for details). Neither method (M06-2X or B3LYP) produced results that were entirely consistent with our experimental findings. Using M06-2X, diastereomer **exo-5** was found to be lower in energy than **endo-5** (the major

diastereomer produced during the experiment). Conversely, when B3LYP was used, diastereomer *endo*-5 was lower in energy, but the magnitude was not entirely consistent with the observed selectivity. These results indicated that the observed selectivity was likely not due to product equilibration;[18] instead, they pointed toward a difference in transition-state structure as the source of the observed selectivity.

2.2.3. Transition-State Structures. Because syn malonate salt **16S** was found to be lower in energy than either anti malonate isomer (section 2.2.1), only transition states arising from **16S** were fully considered.[34] Transition-state calculations (using both M06-2X and B3LYP) for the endo and exo approach were performed with both Na and K counterions. These are shown (for M = K) in Figure 3, along with the final structures optimized using M06-2X. Results from the experiments with Na were quite similar to those with K and can be found in the Supporting Information (Figure S1).
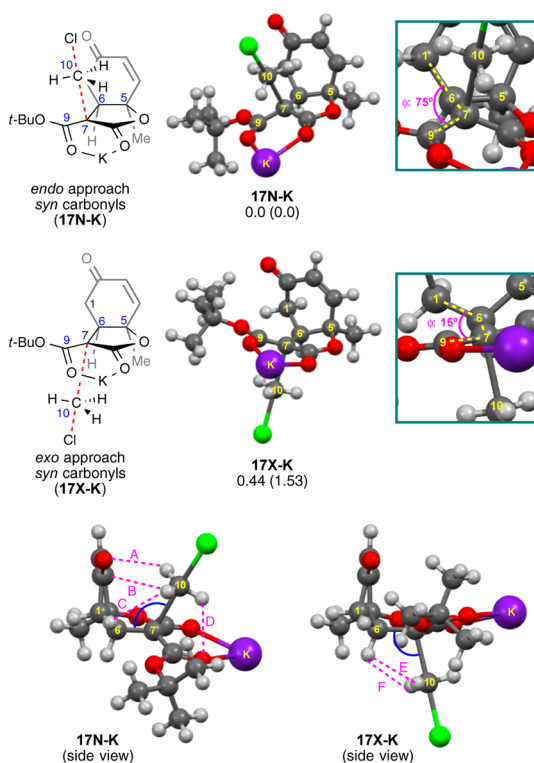

Figure 3. Structure of the calculated transition states incorporating a K counterion. Only structures optimized with M06-2X are shown. Structures calculated using B3LYP can be found in the Supporting Information. Values below the middle structures are relative energies (kcal/mol) calculated with M06-2X (B3LYP). Carbon numbering is the same as that shown in Scheme 5. The blue lines represent the C6−C7−C10 angle. The pink dashed lines represent through-space distances.

Both M06-2X and B3LYP returned endo transitions states (**17N-K**) that were lower in energy than the corresponding exo transition states (**17X-K**). The $\Delta G^{\ddagger}$ obtained with M06-2X (0.44 kcal/mol) was slightly smaller than that obtained with B3LYP (1.53 kcal/mol) and is more consistent with the level of diastereoselectivity observed during the reaction. Closer inspection of the two transition states revealed the basis for their energy difference. As shown in Figure 3 (insets), the C7 carbon atom (the nucleophile) of transition state **17N** is in a staggered orientation. In contrast, the C7 carbon atom in

transition state **17X** is in an eclipsed orientation. This is evidenced by measuring the C9−C7−C6−C1 dihedral angle (Table 5 and Table S2, Supporting Information). In **17N-K**,

Table 5. Selected Measurements of the Transition States Incorporating a K or Na Counterion That Were Calculated Using M06-2X

C7−C10/C10−Cl bond length (Å)			
17N-K	2.243/2.230	**17X-K**	2.207/2.237
17N-Na	2.233/2.246	**17X-Na**	2.194/2.249
C9−C7−C6−C1 dihedral angle (deg)			
17N-K	75.2	**17X-K**	14.6
17N-Na	75.1	**17X-Na**	12.1
C6−C7−C10 angle (deg)			
17N-K	115.0	**17X-K**	103.9
17N-Na	114.7	**17X-Na**	103.5
Through-space distances (Å)			
Distance A (C10H−C3)			
17N-K	2.715	**17N-Na**	2.706
Distance B (C10H−C2)			
17N-K	2.775	**17N-Na**	2.770
Distance C (C10H−C1H)			
17N-K	2.666	**17N-Na**	2.678
Distance D (C10H−O)			
17N-K	2.500	**17N-Na**	2.558
Distance E (C10H−C6H)			
17X-K	2.548	**17X-Na**	2.502
Distance F (C10H−C6H)			
17X-K	2.302	**17X-Na**	2.310

this angle is ∼75° but is only ∼15° in **17X-K**. Similar angles can be found in the transition state of the sodium salt. The compression of this dihedral angle introduces torsional strain into the system, which, in turn, raises the energy of the exo transition states. These observations are quite similar to the "torsional steering" model advanced by Houk and co-workers.[35,36] This model has proven effective for rationalizing the stereoselectivity of several different reaction types, including epoxidation,[37−39] dihydroxylation,[40] Mannich-type reactions,[41] Diels−Alder reactions,[42] iodocyclizations,[43] and Michael additions of β-iminoesters.[44] Torsional effects have also been used to explain[45] the unexpected diastereoselectivity observed by Meyers during α-alkylations of chiral lactams.[46−48]

Even with less torsional strain being present in **17N**, there is still the question of potential steric hindrance during endo approach of the electrophile. One explanation for this is shown at the bottom of Figure 3. Here, the structures of **17N-K** and **17X-K** are rotated 90°. Upon inspection, the C6−C7−C10 bond angle appears to be larger in the endo transition state than in the exo transition state. This is confirmed by the following measurements (Table 5 and Table S2, Supporting Information). In **17X-K**, this angle is ∼104°, whereas, in **17N-K**, this angle is ∼115°. It is plausible that, by entering at a larger angle, the electrophile can not only engage in a staggered transition state but also avoid potential steric clashes with the cyclohexenone ring. Further evidence for this can be found by measuring the closest neighbors to the three hydrogen atoms of C10 (pink dashed lines in Figure 3). In **17N-K**, the closest contact (distance D, 2.50 Å) is between the C10 hydrogen atom and one of the malonate oxygen atoms (Table 5 and Table S2, Supporting Information). There are also contacts between the C10 hydrogen atoms and C3 and C2 (distances A

and B) that are closer than the sum of the Van der Waal radii (2.9 Å).[49] Distance C, between one C10−H and C1−H, is outside the sum of the Van der Waal radii for two hydrogen atoms (2.4 Å)[49] and is likely unimportant. All other measurements from the C10 hydrogen atoms are >2.8 Å. In contrast, with **17X-K**, there are close contacts between two C10 hydrogen atoms and the C6 hydrogen atom (2.30−2.55 Å). In both cases, these distances are shorter than those found in endo transition states. The distance between the C10−H and the malonate oxygen atoms in **17X-K** (2.725 and 2.729 Å, not shown) is slightly larger than the sum of the Van der Waal radii (∼2.7 Å)[49] and is likely unimportant. Overall, this analysis implies that, with a small electrophile like MeI, the endo transition state is favored on both torsional and steric (through-space) grounds.

These same measurements also explain why electrophiles larger than MeI prefer an exo approach (Table 3). Clearly, any extended carbon chain on C10 will orient itself away from the cyclohexenone ring during the endo approach. However, the C6−C7−C10 bond angle preferred by transition state **17N** means that any extended carbon chain will be oriented toward the exocyclic ester of the malonate nucleophile. Alternatively, approach from the exo direction will allow the carbon chain to be oriented away from the exocyclic ester. Thus, larger electrophiles will experience decreased through-space steric interactions when engaging the malonate anion from an exo approach, compensating for the energetic cost associated with the torsional strain of the exo transition state.

What is not adequately addressed by our calculations is the observed influence on the diastereoselectivity by solvent (Table 1). As stated before, the observed selectivity does not correlate well with solvent polarity. More specifically, reactions performed in ethereal solvents demonstrated greatly diminished endo selectivity, regardless of their polarity. This is likely related to the Lewis basic nature of the oxygen atoms that are necessarily present. One possible explanation is that coordination of the solvent to the metal cation in **16S** creates a solvent shell that blocks access to the endo face of the malonate. While a coordinated solvent shell is certainly possible with acetonitrile, the shape of the shell formed will be quite different. This difference is related to the hybridization of the Lewis basic atoms involved. Coordination of a linear acetonitrile through an sp-hybridized nitrogen would result in a solvent shell that is shaped much differently from that formed by coordination of an ether molecule through an sp^3-hybridized oxygen atom.

Another possibility is that relative differences in Lewis basicity between the various solvents[50] are able to influence the coordination of the malonate anion to the metal cation, and any solvent shell that accompanies it. Some evidence for this can be found with our experiments in the presence of known metal chelators. For instance, when 18-crown-6 was used with K_2CO_3, the endo selectivity increased (Table 2, entries 7 and 8). Similarly, adding increasing amounts of HMPA also results in increased endo selectivity in THF (Table 2, compare entries 9 and 10). Given the small energy differences involved and the inherent errors associated with solvation models,[51] using computational methods to rationalize our observations does not seem to be reasonable at this time.[52] Moreover, testing the hypotheses proposed above would likely require the use of explicit (atomistic) solvent molecules, which would significantly increase the computational cost.

2.3. Further Experimental Results. ### 2.3.1. Comparison with Literature Examples.

The computational results described above have uncovered several factors that influence the stereochemical outcome of alkylation reactions involving cyclohexadienone-derived bicyclic malonates. However, they do not fully explain why our results with MeI differ so much from the literature reports on similar alkylations, selected examples[13−15] of which are shown in eqs 1−4. While details regarding the diastereoselectivity cannot be found with all of these literature examples, they are all overwhelmingly exoselective.
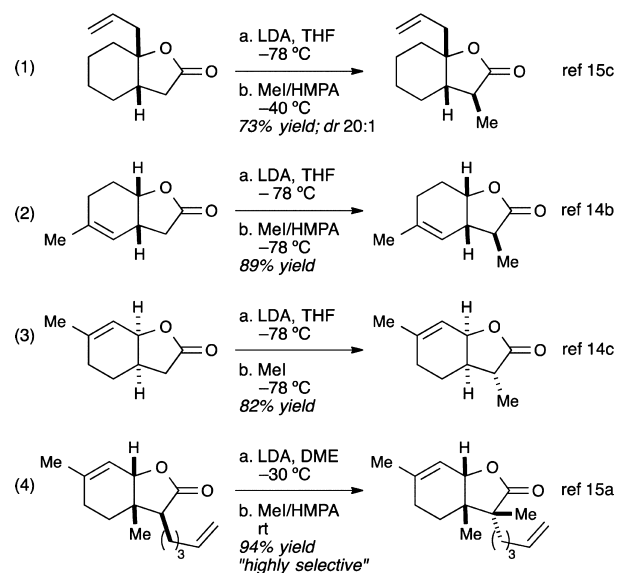
There are two aspects of these reactions that might contribute to their exo preference. First, all of the literature examples were performed with LDA in ethereal solvents. Unfortunately, lithium bases were not successful in promoting our alkylation reaction (Table 2), so at this time, we can only speculate on the influence of the lithium cation. However, we have found that ethereal solvents have a profound influence on the diastereoselectivity (Table 1). More specifically, they lead to more exo selective reactions.

The second potentially important difference between our alkylation and the literature examples is a structural one. Comparing **6** and the conjugate acid of **2** to the literature examples reveals that ours is the only system with three sp^2 carbons in the six-membered ring. This imparts a great deal of planarity to the ring. In contrast, the extra sp^3 carbons present in the literature reports (eqs 1−4) would be expected to increase steric interactions between a methyl group approaching the enolate from the concave face and the six-membered ring (i.e., shorten distance A and/or B in Figure 3). It stands to reason that adding even one more sp^3-hybridized carbon atom to the six-membered ring would increase steric interactions with the incoming electrophile to such an extent that they can override the torsional strain associated with the exo approach. Houk and co-workers have found that steric control can outweigh torsional steering during the alkylation of certain substrates.[53]

2.3.2. Manipulating the Steric Environment.

The level of diastereoselectivity observed during the studied alkylation reactions suggest that the difference between the energetic gains afforded by a staggered transition state and the unfavorable sterics of an endo approach are quite small. This

is supported by the free energy differences obtained from our calculations. These results, coupled with the ability to manipulate the steric environment of an α,β-unsaturated ketone, suggest that the structure of our substrates can be manipulated to override the inherent stereoselectivity observed with MeI.

This hypothesis was tested, as shown in Scheme 6. Enone **6** was hydrogenated with Pd/C to provide cyclohexanone **18**.

Scheme 6
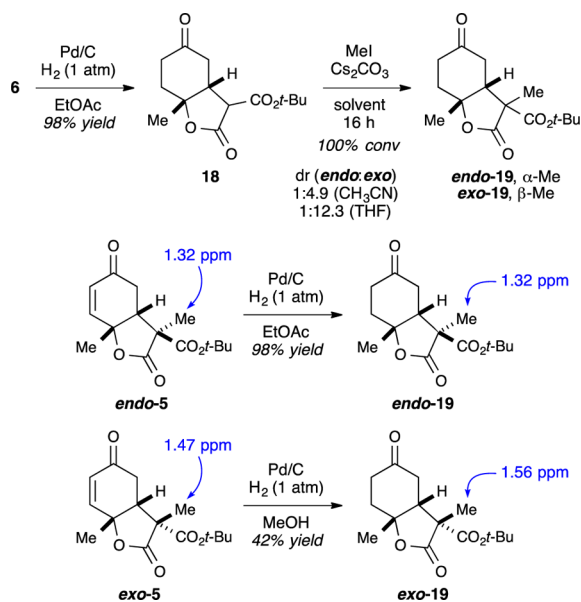
The malonate in **18** was then alkylated to afford an inseparable mixture of **endo-19** and **exo-19**. The structural assignment of the alkylated products was accomplished by comparing the chemical shifts of the methyl groups in **endo-19** and **exo-19** with those of the methyl groups in **endo-5** and **exo-5**. This assignment was confirmed by hydrogenating purified samples of **endo-5** and **exo-5**. Gratifyingly, when the alkylation of **18** was performed in acetonitrile, a diastereomeric ratio of 4.9:1 favoring **exo-19** was observed. Interestingly, when the solvent was changed to THF, the diastereoselectivity increased to 12.3:1, again favoring **exo-19**. The finding that the alkylation of saturated ketone **18** with MeI is selective for the exo diastereomer confirms that the enone in **6** (and by extension **2**) plays an important role in making the endo approach accessible to small electrophiles.

3. CONCLUSIONS

Our studies have revealed the origin for the endo selectivity observed during alkylation reactions of cyclohexadienone-derived bicyclic malonates with MeI. This result can be traced to an energetically favorable endo transition state that experiences less torsional strain. This is in line with the torsional steering model advanced by Houk and co-workers. However, the line between the favorable energetics offered by a staggered transition state and unfavorable steric interactions is razor thin. With even a modest increase in electrophile size, the steric penalties accrued during an endo trajectory are such that they force the electrophile to take an exo approach. Similar steric arguments can be used to explain why our observed diastereomeric ratios with MeI differ significantly from literature examples with otherwise very similar substrates.

These arguments are related to the planarity and rigidity that arise from replacing one sp^3 carbon (in the literature cases) with an sp^2 carbon (in the present case) in a fused 5,6 ring system. This slight decrease in steric crowding is seemingly sufficient to provide access to the energetically favorable endo transition state.

Finally, we have shown that the steric environment of these substrates can be modified by harnessing the reactivity of the enone moiety. In this case, hydrogenation of the C−C double bond can be used to overcome the endo selectivity observed with enone **6**. While this specific approach will not provide direct access to the originally targeted vinylogous ester **exo-3**, it sets the stage for developing a strategy in which the steric environment of the substrate is temporarily modified to allow for an exo selective alkylation event. The development of such a strategy is underway[54] and will be reported in due course.

4. EXPERIMENTAL SECTION

4.1. Computational Methods. All calculations were performed using the Gaussian 09, Rev. C.01, suite[55] of electronic structure programs. All geometries were fully optimized at both the M06-2X[20] and B3LYP[21] levels using the 6-31G(d)[22] basis set. An ultrafine grid density was used for numerical integration.[56] Optimizations were performed with no frozen coordinates. To account for solvation effects, the SMD solvation model[51] for acetonitrile was employed during geometry optimizations. Energy minima and transition states were identified through frequency analysis. The Gibbs energies for all relevant species can be found in the Supporting Information (Table S1).

To account for conformational flexibility with the exocyclic ester of **endo-5** and **exo-5**, a relaxed scan of the C6−C7−C9−O dihedral was performed. A full 360° scan was performed in 11 steps (30° intervals), and the geometry of the molecule was optimized at each interval. Relative energy plots for each scan can be found in the Supporting Information. With **exo-5**, there were two conformers within 1 kcal of each other. Both were used to calculate the free energy differences given in Figure 2, which is why an energy range is reported. The Gibbs energy and coordinates for all relevant minima (one for **endo-5**, two for **exo-5**) are reported in the Supporting Information.

Houk and co-workers have found that the conformation of cyclopentene rings can be crucial for the torsional effects we are observing.[40] Conformational analysis of the two envelope conformations of the lactone enolate for **16S**, **17N**, and **17X** (M = Na and K) were performed. The two conformations of **16S** were within 1 kcal/mol of each other, but the transition states leading from these alternate conformations were both higher in energy than those shown in Figure 3. The details of this analysis can be found in the Supporting Information.

4.2. Materials and Methods. Unless otherwise stated, reactions were performed in screw cap vials under ambient conditions. Acetonitrile, CH$_2$Cl$_2$, MTBE, and DME were dried by passage through an activated alumina column under argon. Tetrahydrofuran, dioxane, and diethyl ether were distilled from sodium/benzophenone. Thin-layer chromatography (TLC) was performed using plates precoated with silica gel XHL w/UV254 (250 mm) and visualized by UV light or KMnO$_4$ stain, followed by heating. All necessary purifications were conducted by flash column chromatography (FCC) using silica gel (particle size 32−63 mm). ^{1}H and ^{13}C NMR spectra are reported relative to the residual solvent peak (δ 7.26 and δ 77.2 for ^{1}H and ^{13}C, respectively). Data for ^{1}H NMR spectra are reported as follows: chemical shift (δ (ppm)) (multiplicity, coupling constant (Hz), integration). Spectra are described using the following abbreviations: s = singlet, d = doublet, t = triplet, q = quartet, m = multiplet. IR samples were prepared on NaCl plates by evaporation from CHCl$_3$ or CH$_2$Cl$_2$. HPLC analysis was performed using an Agilent Technologies ZORBAX Eclipse XDB-CN column (4.6 × 150 mm, 3.5 μm) with a diode array detector with a mercury lamp (λ = 225 nm unless otherwise noted). For all compounds, the mobile phase

consisted of 5% isopropanol in hexanes (isocratic) with a flow rate of 1 mL/min.

4.3. Sample Preparation. Samples requiring quantitative NMR (qNMR) yields and diastereomeric ratios were prepared by diluting the reaction mixture with EtOAc, filtering the mixture over a plug of silica, adding Ph₃CH as an internal standard, and concentrating. Reaction mixtures containing THF, DME, acetone, or MTBE were first concentrated before being diluted with EtOAc. Reaction mixtures containing dioxane, DMF, or HMPA were subjected to an aqueous workup and extracted with EtOAc (3×). The combined organic layers were washed with H₂O and brine, dried (Na₂SO₄), filtered, and then treated with the internal standard (Ph₃CH) before being concentrated. In all cases, the entire crude mixture was taken up in CDCl₃ and the yield determined by qNMR. The sample was then concentrated and diluted with isopropanol/hexanes for HPLC analysis. Diastereomers were separated by FCC (20% EtOAc in hexanes) and characterized individually.

4.4. General Procedure for Alkylation. The substrate (0.131 mmol) was weighed into a 1 dram vial and dissolved in solvent (0.08 M). Base (1.2 equiv, 0.157 mmol) was then added to this mixture, followed by the electrophile (1.2 equiv, 0.157 mmol). The reaction mixture was stirred at rt for 8−16 h. For reactions using compound **6** as the starting material, the reaction progress was monitored by HPLC. After such time, the mixture was diluted with EtOAc, filtered over a plug of silica, and concentrated.

4.5. Procedure for the One-Pot Cyclization/Alkylation of 4. Malonate-tethered cyclohexadienone **4** (35.2 mg, 0.131 mmol) was stirred in acetonitrile (1.6 mL). Cs₂CO₃ (90.0 mg, 0.276 mmol) was added, followed by iodomethane (9 μL). The reaction progress was followed using TLC to monitor the disappearance of the UV-active starting material as the product is not UV-active, but stains with KMnO₄ (both starting material and product have the same R_f). The mixture was stirred for 16 h at rt, then diluted with EtOAc (2 mL) and filtered over a plug of silica, eluting with EtOAc. The internal standard (Ph₃CH) was added, and the mixture was concentrated under reduced pressure. Compound **5** was obtained in 83% yield (30.6 mg) for both diastereomers. The diastereomers were separated by FCC (20% EtOAc in hexanes).

4.6. Procedure for Alkylation of 6 with Chloromethane. Chloromethane (450 mg) was condensed into a pressure tube that was cooled to −78 °C. Acetonitrile (1.6 mL), substrate **6** (35.6 mg, 0.134 mmol), and Cs₂CO₃ (51.3 mg, 0.158 mmol) were added quickly, and the tube was capped, allowed to warm to rt, and stirred overnight. After 24 h, the cap was removed and the mixture was concentrated under a stream of nitrogen. The residue was diluted with EtOAc and filtered over a plug of silica. The internal standard was added, and the mixture was concentrated under reduced pressure.

Compounds **1**,[11] **3**,[11] **4**,[16] **6**,[16] **10**,[16] and **12**[16] have previously been synthesized. HPLC retention times (t_R) are reported for **3** and **6**.

4.7. (3R*,3aS*,7aR*)-tert-Butyl 7-Methoxy-3,6,7a-trimethyl-2,5-dioxo-2,3,3a,4,5,7a-hexahydrobenzofuran-3-carboxylate (endo-3): HPLC t_R = 6.6 min (λ = 254 nm).

4.8. (3R*,3aR*,7aR*)-tert-Butyl 7-Methoxy-3,6,7a-trimethyl-2,5-dioxo-2,3,3a,4,5,7a-hexahydrobenzofuran-3-carboxylate (exo-3): HPLC t_R = 8.9 min (λ = 254 nm).

4.9. (3R*,3aS*,7aR*)-tert-Butyl 3,7a-Dimethyl-2,5-dioxo-2,3,3a,4,5,7a-hexahydrobenzofuran-3-carboxylate (endo-5): Beige amorphous solid (24.0 mg, 65%). ¹H NMR (500 MHz, CDCl₃) δ 6.72 (dd, J = 10.4, 1.2 Hz, 1H), 6.06 (d, J = 10.4 Hz, 1H), 3.38 (ddd, J = 6.9, 2.5, 1.3 Hz, 1H), 2.70 (dd, J = 18.2, 6.9 Hz, 1H), 2.59 (dd, J = 18.2, 2.5 Hz, 1H), 1.70 (s, 3H), 1.46 (s, 9H), 1.32 (s, 3H); ¹³C NMR (125 MHz, CDCl₃, DEPT) δ 194.9 (C), 173.9 (C), 169.2 (C), 147.7 (CH), 129.4 (CH), 83.4 (C), 79.5 (C), 55.8 (C), 47.6 (CH), 34.5 (CH₂), 27.9 (CH₃ × 3), 26.5 (CH₃), 16.0 (CH₃); HRMS (ESI-TOF) m/z calcd for C₁₅H₂₀O₅Na [M + Na]⁺ 303.1203, found 303.1198; HPLC t_R = 9.7 min; TLC R_f 0.4 (3:1 hexanes/EtOAc).

4.10. (3R*,3aR*,7aR*)-tert-Butyl 3,7a-Dimethyl-2,5-dioxo-2,3,3a,4,5,7a-hexahydrobenzofuran-3-carboxylate (exo-5): White amorphous solid (4.4 mg, 12%). ¹H NMR (500 MHz,

CDCl₃) δ 6.72 (dd, J = 10.4, 1.6 Hz, 1H), 5.93 (d, J = 10.4 Hz, 1H), 3.00−2.95 (m, 1H), 2.69−2.63 (m, 2H), 1.64 (s, 3H), 1.47 (s, 3H), 1.34 (s, 9H); ¹³C NMR (125 MHz, CDCl₃, DEPT) δ 193.3 (C), 173.6 (C), 168.6 (C), 147.4 (CH), 129.6 (CH), 84.6 (C), 79.2 (C), 55.0 (C), 51.8 (CH), 33.3 (CH₂), 27.7 (CH₃ × 3), 26.1 (CH₃), 21.6 (CH₃); IR 2979, 2937, 1787, 1728, 1679 cm⁻¹; HRMS (ESI-TOF) m/z calcd for C₁₅H₂₀O₅Na [M + Na]⁺ 303.1203, found 303.1204; HPLC t_R = 13.9 min; TLC R_f 0.2 (3:1 hexanes/EtOAc).

4.11. (3R*,3aS*,7aS*)-tert-Butyl 7a-Methyl-2,5-dioxo-2,3,3a,4,5,7a-hexahydrobenzofuran-3-carboxylate (6): The synthesis and characterization of compound **6** has previously been reported.[16] HPLC t_R = 8.3 min.

4.12. (3R*,3aR*,7aR*)-tert-Butyl 3-Benzyl-7a-methyl-2,5-dioxo-2,3,3a,4,5,7a-hexahydrobenzofuran-3-carboxylate (7): Isolated a white amorphous solid after purification by FCC (41.7 mg, 89% yield). ¹H NMR (500 MHz, CDCl₃) δ 7.33−7.27 (m, 3H), 7.22 (d, J = 6.8 Hz, 2H), 6.69 (dd, J = 10.4, 1.6 Hz, 1H), 5.95 (d, J = 10.4 Hz, 1H), 3.44 (d, J = 14.1 Hz, 1H), 3.09 (d, J = 14.1 Hz, 1H), 2.97 (d, J = 18.5 Hz, 1H), 2.69 (d, J = 7.7 Hz, 1H), 2.57 (dd, J = 18.5, 7.7 Hz, 1H), 1.37 (s, 9H), 1.36 (s, 3H); ¹³C NMR (125 MHz, CDCl₃, DEPT) δ 193.4 (C), 172.6 (C), 168.3 (C), 147.5 (CH), 134.7 (C), 130.9 (CH × 2), 129.6 (CH), 128.9 (CH × 2), 127.7 (CH), 85.0 (C), 79.1 (C), 60.5 (C), 45.7 (CH), 38.8 (CH₂), 33.0 (CH₂), 27.7 (CH₃ × 3), 26.0 (CH₃); IR 2979, 2930, 1783, 1726, 1685 cm⁻¹; HRMS (ESI-TOF) m/z calcd for C₂₁H₂₄O₅Na [M + Na]⁺ 379.1516, found 379.1524; HPLC t_R = 9.3 min; TLC R_f 0.5 (3:1 hexanes/EtOAc).

4.13. (3R*,3aR*,7aR*)-tert-Butyl 3-Isopropyl-7a-methyl-2,5-dioxo-2,3,3a,4,5,7a-hexahydrobenzofuran-3-carboxylate (8): Isolated a beige amorphous solid after purification by FCC (7.7 mg, 19% yield). ¹H NMR (500 MHz, CDCl₃) δ 6.70 (dd, J = 10.4, 1.7 Hz, 1H), 5.95 (d, J = 10.4 Hz, 1H), 3.04 (d, J = 18.6 Hz, 1H), 2.91 (d, J = 7.6 Hz, 1H), 2.63 (dd, J = 18.6, 7.5 Hz, 1H), 2.22 (qq, J = 6.8, 6.8 Hz, 1H), 1.65 (s, 3H), 1.39 (s, 9H), 1.16 (d, J = 6.8 Hz, 3H), 1.10 (d, J = 6.8 Hz, 3H); ¹³C NMR (125 MHz, CDCl₃, DEPT) δ 193.6 (C), 171.9 (C), 167.9 (C), 147.6 (CH), 129.7 (CH), 84.7 (C), 78.4 (C), 61.4 (C), 46.7 (CH), 33.9 (CH₂), 33.0 (CH), 27.8 (CH₃ × 3), 26.1 (CH₃), 18.0 (CH₃), 17.7 (CH₃); IR 2977, 2934, 1782, 1724, 1685 cm⁻¹; HRMS (ESI-TOF) m/z calcd for C₁₇H₂₄O₅Na [M + Na]⁺ 331.1516, found 331.1514; TLC R_f 0.3 (3:1 hexanes/EtOAc).

4.14. (3R*,3aR*,7aR*)-tert-Butyl 3-Allyl-7a-methyl-2,5-dioxo-2,3,3a,4,5,7a-hexahydrobenzofuran-3-carboxylate (9): Two fractions were isolated after purification by FCC. The first contained two diastereomers (beige solid, 14.4 mg), and the second contained one diastereomer (white solid, 18.7 mg) for a combined isolated yield of 81% (32.7 mg). Only the major diastereomer was characterized. ¹H NMR (500 MHz, CDCl₃) δ 6.72 (dd, J = 10.4, 1.9 Hz, 1H), 5.95 (dd, J = 10.4, 0.8 Hz, 1H), 5.82 (dddd, J = 16.9, 10.2, 8.1, 6.7 Hz, 1H), 5.24−5.16 (m, 2H), 2.94 (dt, J = 18.6, 1.1 Hz, 1H), 2.84 (dt, J = 7.5, 1.6 Hz, 1H), 2.72−2.67 (m, 1H), 2.61 (dd, J = 18.6, 7.5 Hz, 1H), 2.51 (dd, J = 14.1, 8.1 Hz, 1H), 1.63 (s, 3H), 1.36 (s, 9H); ¹³C NMR (125 MHz, CDCl₃, DEPT) δ 193.4 (C), 172.4 (C), 167.9 (C), 147.5 (CH), 131.5 (CH), 129.6 (CH), 121.4 (CH₂), 84.9 (C), 79.3 (C), 58.3 (C), 47.3 (CH), 38.5 (CH₂), 33.2 (CH₂), 27.7 (CH₃ × 3), 26.0 (CH₃); IR 2979, 2932, 1784, 1724, 1685 cm⁻¹; HRMS (ESI-TOF) m/z calcd for C₁₇H₂₂O₅Na [M + Na]⁺ 329.1350, found 329.1361.

4.15. (3R*,3aS*,7aS*)-Benzyl 3,7a-Dimethyl-2,5-dioxo-2,3,3a,4,5,7a-hexahydrobenzofuran-3-carboxylate (endo-11): Pale yellow amorphous solid (14.6 mg, 71% yield). ¹H NMR (500 MHz, CDCl₃) δ 7.39−7.33 (m, 5H), 6.75 (dd, J = 10.4, 1.5 Hz, 1H), 6.08 (d, J = 10.4 Hz, 1H), 5.22 (s, 2H), 3.42 (dt, J = 6.9, 1.8 Hz, 1H), 2.68 (dd, J = 18.3, 7.0 Hz, 1H), 2.61 (dd, J = 18.2, 1.6 Hz, 1H), 1.69 (s, 3H), 1.43 (s, 3H); ¹³C NMR (125 MHz, CDCl₃, DEPT) δ 194.6 (C), 173.3 (C), 170.1 (C), 147.6 (CH), 135.1 (C), 129.5 (CH), 128.8 (CH × 2), 128.7 (CH), 128.1 (CH × 2), 79.8 (C), 68.2 (CH₂), 55.3 (C), 47.5 (CH), 34.4 (CH₂), 26.5 (CH₃), 16.1 (CH₃); IR 3035, 2949, 1778, 1738, 1686 cm⁻¹; HRMS (ESI-TOF) m/z calcd for C₁₈H₁₈O₅Na [M + Na]⁺ 337.1046, found 337.1052; HPLC t_R = 17.2 min.

4.16. (3R*,3aR*,7aR*)-Benzyl 3,7a-Dimethyl-2,5-dioxo-2,3,3a,4,5,7a-hexahydrobenzofuran-3-carboxylate (exo-11):

White amorphous solid (1.8 mg, 9% yield). ^{1}H NMR (500 MHz, CDCl$_3$) δ 7.36−7.30 (m, 5H), 6.55 (dd, J = 10.4, 1.9 Hz, 1H), 5.60 (d, J = 10.4 Hz, 1H), 5.07 (d, J = 12.2 Hz, 1H), 4.91 (d, J = 12.2 Hz, 1H), 2.99 (d, J = 18.1 Hz, 1H), 2.73−2.72 (m, 1H), 2.67 (dd, J = 18.1, 7.3 Hz, 1H), 1.65 (s, 3H), 1.55 (s, 3H); ^{13}C NMR (125 MHz, CDCl$_3$, DEPT) δ 192.9 (C), 173.3 (C), 169.5 (C), 147.2 (CH), 128.9 (CH), 128.80 (CH × 4), 128.79 (CH), 79.5 (C), 67.9 (CH$_2$), 54.1 (C), 52.4 (CH), 33.4 (CH$_2$), 25.9 (CH$_3$), 21.3 (CH$_3$); HRMS (ESI-TOF) m/z calcd for C$_{18}$H$_{18}$O$_5$Na [M + Na]$^+$ 337.1046, found 337.1044; HPLC t_R = 24.1 min.

4.17. (3R*,3aS*,7aR*)-tert-Butyl 3,7,7a-Trimethyl-2,5-dioxo-2,3,3a,4,5,7a-hexahydrobenzofuran-3-carboxylate (endo-13): White amorphous solid (40.1 mg, 50% yield). ^{1}H NMR (500 MHz, CDCl$_3$) δ 5.92 (s, 1H), 3.38 (dd, J = 7.3, 1.8 Hz, 1H), 2.68 (dd, J = 18.4, 7.3 Hz, 1H), 2.60−2.56 (m, 1H), 2.04 (d, J = 1.4 Hz, 3H), 1.72 (s, 3H), 1.45 (s, 9H), 1.30 (s, 3H); ^{13}C NMR (125 MHz, CDCl$_3$, DEPT) δ 194.5 (C), 173.9 (C), 161.2 (C), 158.6 (C), 128.0 (CH), 83.3 (C), 81.7 (C), 55.5 (C), 48.5 (CH), 34.1 (CH$_2$), 27.9 (CH$_3$ × 3), 25.5 (CH$_3$), 18.7 (CH$_3$), 16.0 (CH$_3$); IR 2981, 2935, 1780, 1734, 1676 cm^{-1}; HRMS (ESI-TOF) m/z calcd for C$_{16}$H$_{22}$O$_5$Na [M + Na]$^+$ 317.1359, found 317.1353; HPLC t_R = 8.2 min.

4.18. (3R*,3aR*,7aR*)-tert-Butyl 3,7,7a-Trimethyl-2,5-dioxo-2,3,3a,4,5,7a-hexahydrobenzofuran-3-carboxylate (exo-13): Pale yellow amorphous solid (14.0 mg, 17% yield). ^{1}H NMR (500 MHz, CDCl$_3$) δ 5.80 (s, 1H), 3.00−2.95 (m, 1H), 2.68−2.63 (m, 2H), 2.05 (d, J = 1.3 Hz, 3H), 1.67 (s, 3H), 1.47 (s, 3H), 1.36 (s, 9H); ^{13}C NMR (125 MHz, CDCl$_3$, DEPT) δ 193.1 (C), 173.7 (C), 168.7 (C), 158.8 (C), 128.2 (CH), 84.5 (C), 81.5 (C), 54.6 (C), 52.6 (CH), 33.1 (CH$_2$), 27.6 (CH$_3$ × 3), 25.2 (CH$_3$), 21.1 (CH$_3$), 18.5 (CH$_3$); HRMS (ESI-TOF) m/z calcd for C$_{16}$H$_{22}$O$_5$Na [M + Na]$^+$ 317.1359, found 317.1359; HPLC t_R = 12.0 min.

4.19. (3R*,3aS*,7aR*)-tert-Butyl 7-Methoxy-6,7a-dimethyl-2,5-dioxo-2,3,3a,4,5,7a-hexahydrobenzofuran-3-carboxylate (14): Substrate **14** was synthesized from the previously reported malonate-tethered cyclohexadienone **1**^{11} in the same manner as compound **6**. Crude residue was purified by FCC and isolated as an amorphous white solid (320 mg, 87% yield). ^{1}H NMR (500 MHz, CDCl$_3$) δ 3.95 (s, 3H), 3.33 (d, J = 12.3 Hz, 1H), 3.20 (ddd, J = 12.3, 5.3, 2.5 Hz, 1H), 2.68 (dd, J = 17.5, 5.4 Hz, 1H), 2.62 (dd, J = 17.5, 2.5 Hz, 1H), 1.78 (s, 3H), 1.77 (s, 3H), 1.48 (s, 9H); ^{13}C NMR (125 MHz, CDCl$_3$, DEPT) δ 195.1 (C), 169.4 (C), 166.4 (C), 165.4 (C), 121.2 (C), 83.8 (C), 82.6 (C), 61.3 (CH), 52.0 (CH), 44.1 (CH), 35.7 (CH$_2$), 28.0 (CH$_3$ × 3), 22.9 (CH$_3$), 9.1 (CH$_3$); IR 2989, 2933, 1784, 1734, 1650, 1610 cm^{-1}; HRMS (ESI-TOF) m/z calcd for C$_{16}$H$_{22}$O$_6$Na [M + Na]$^+$ 333.1309, found 333.1321; HPLC t_R = 6.5 min ($λ$ = 254 nm); TLC R_f 0.4 (3:1 hexanes/EtOAc).

4.20. (3R*,3aS*,7aS*)-tert-Butyl 7a-Methyl-2,5-dioxooctahydrobenzofuran-3-carboxylate (18): Prepared by hydrogenation of **6** (127 mg, 0.477 mmol) using Degussa Pd/C (Type E101 Ne/W, obtained from Sigma-Aldrich, 98 mg) in EtOAc (5 mL) with a balloon of H$_2$ (1 atm) at rt for 1 h. The reaction mixture was filtered over a pad of Celite and concentrated under reduced pressure. An amorphous white solid was isolated (126 mg, 98% yield). No further purification was necessary. ^{1}H NMR (500 MHz, CDCl$_3$) δ 3.22 (d, J = 7.7 Hz, 1H), 3.08 (td, J = 7.0, 4.3 Hz, 1H), 2.63 (dd, J = 16.2, 6.4 Hz, 1H), 2.41 (dd, J = 16.3, 4.1 Hz, 1H), 2.32 (tdd, J = 18.5, 10.1, 5.2 Hz, 2H), 2.19−2.07 (m, 2H), 1.63 (s, 3H), 1.46 (s, 10H); ^{13}C NMR (125 MHz, CDCl$_3$, DEPT) δ 208.5 (C), 170.0 (C), 166.1 (C), 83.6 (C), 83.4 (C), 54.7 (CH), 43.1 (CH), 41.1 (CH$_2$), 35.1 (CH$_2$), 33.0 (CH$_2$), 27.9 (CH$_3$ × 3), 27.3 (CH$_3$); IR 2978, 2935, 1771, 1727 cm^{-1}; HRMS (ESI-TOF) m/z calcd for C$_{14}$H$_{20}$O$_5$Na [M + Na]$^+$ 291.1203, found 291.1200.

4.21. (3R*,3aR*,7aS*)-tert-Butyl 3-Benzyl-7-methoxy-6,7a-dimethyl-2,5-dioxo-2,3,3a,4,5,7a-hexahydrobenzofuran-3-carboxylate (exo-15): White amorphous solid after purification by FCC (41.2 mg, 92% yield). ^{1}H NMR (500 MHz, CDCl$_3$) δ 7.32−7.21 (m, 5H), 3.96 (s, 3H), 3.41 (d, J = 14.1 Hz, 1H), 3.09 (d, J = 14.1 Hz, 1H), 3.00 (d, J = 16.6 Hz, 1H), 2.60−2.53 (m, 2H), 1.72 (s, 3H), 1.43 (s, 3H), 1.34 (s, 9H); ^{13}C NMR (75 MHz, CDCl$_3$, DEPT) δ 194.2 (C), 172.7 (C), 168.2 (C), 167.1 (C), 134.6 (C), 130.9 (CH × 2), 128.9

(CH × 2), 127.7 (CH), 121.2 (C), 84.8 (C), 81.2 (C), 61.0 (CH3), 60.4 (C), 45.3 (CH), 38.6 CH$_2$), 32.8 (CH$_2$), 27.7 (CH$_3$ × 3), 25.2 (CH$_3$), 9.1 (CH$_3$); IR 2980, 2929, 1790, 1729, 1668 cm^{-1}; HRMS (ESI-TOF) m/z calcd for C$_{23}$H$_{28}$O$_6$Na [M + Na]$^+$ 423.1778, found 423.1785; TLC R_f 0.4 (3:1 hexanes/EtOAc).

4.22. (3R*,3aS*,7aS*)-tert-Butyl 3,7a-Dimethyl-2,5-dioxooctahydrobenzofuran-3-carboxylate (endo-19): Prepared by hydrogenation of **endo-5** (42.1 mg, 0.1502 mmol) in the same fashion as **18**. An amorphous beige solid (41.5 mg, 98% yield) was isolated. No further purification was necessary. ^{1}H NMR (500 MHz, CDCl$_3$) δ 3.00 (t, J = 6.8 Hz, 1H), 2.48−2.41 (m, 2H), 2.32 (ddd, J = 16.1, 8.0, 5.1 Hz, 2H), 2.20 (ddd, J = 14.4, 7.3, 5.2 Hz, 1H), 2.11 (ddd, J = 14.3, 9.0, 5.1 Hz, 1H), 1.58 (s, 3H), 1.46 (s, 9H), 1.32 (s, 3H); ^{13}C NMR (125 MHz, CDCl$_3$, DEPT) δ 209.5 (C), 174.5 (C), 170.4 (C), 83.6 (C), 82.6 (C), 55.7 (C), 45.8 (CH), 38.6 (CH$_2$), 34.7 (CH$_2$), 33.1 (CH$_2$), 27.8 (CH$_3$ × 3), 27.5 (CH$_3$), 17.3 (CH$_3$); IR 2978, 2936, 1771, 1719 cm^{-1}; HRMS (ESI-TOF) m/z calcd for C$_{15}$H$_{22}$O$_5$Na [M + Na]$^+$ 305.1359, found 305.1392.

4.23. (3R*,3aR*,7aR*)-tert-Butyl 3,7a-Dimethyl-2,5-dioxooctahydrobenzofuran-3-carboxylate (exo-19): Prepared by hydrogenation of **exo-5** (35.5 mg, 0.127 mmol) in the same fashion as **18** except MeOH was used instead of EtOAc. Product was purified via FCC, and an amorphous beige solid (15.0 mg, 42% yield) was isolated. ^{1}H NMR (500 MHz, CDCl$_3$) δ 2.57−2.46 (m, 4H), 2.39−2.27 (m, 2H), 2.02 (ddd, J = 13.3, 9.4, 3.8 Hz, 1H), 1.61 (s, 3H), 1.56 (s, 3H), 1.44 (s, 9H); ^{13}C NMR (125 MHz, CDCl$_3$, DEPT) δ 207.8 (C), 175.3 (C), 168.4 (C), 84.9 (C), 82.0 (C), 56.8 (C), 50.3 (CH), 38.8 (CH$_2$), 35.0 (CH$_2$), 32.7 (CH$_2$), 29.1 (CH$_3$), 27.7 (CH$_3$ × 3), 24.4 (CH$_3$); HRMS (ESI-TOF) m/z calcd for C$_{15}$H$_{22}$O$_5$Na [M + Na]$^+$ 305.1359, found 305.1366

■ ASSOCIATED CONTENT

Ⓢ Supporting Information

Optimized geometries and energies of all computed species, energy plots for the relaxed scan, and NMR spectra for all new compounds. This material is available free of charge via the Internet at http://pubs.acs.org.

■ AUTHOR INFORMATION

Corresponding Author

*E-mail: harned@umn.edu.

Notes

The authors declare no competing financial interest.

■ ACKNOWLEDGMENTS

■ REFERENCES

(1) Gawley, R. E.; Aubé, J. *Principles of Asymmetric Synthesis*, 2nd ed.; Elsevier: Amsterdam, 2012.

(2) Carreira, E. M.; Kvaerno, L. *Classics in Stereoselective Synthesis*; Wiley-VCH: Weinheim, Germany, 2009.

(3) Hoveyda, A. H.; Evans, D. A.; Fu, G. C. *Chem. Rev.* **1993**, *93*, 1307.

(4) Ho, T.-L. *Stereoselectivity in Synthesis*; Wiley: New York, 1999.

(5) Mengel, A.; Reiser, O. *Chem. Rev.* **1999**, *99*, 1191.

(6) O'Brien, A. G. *Tetrahedron* **2011**, *67*, 9639.

(7) Harned, A. M.; Volp, K. A. *Nat. Prod. Rep.* **2011**, *28*, 1790.

(8) Bringmann, G.; Lang, G.; Mühlbacher, J.; Schaumann, K.; Steffens, S.; Rytik, P. G.; Hentschel, U.; Morschhäuser, J.; Müller, W. E. G.; Sorbicillactone, A. A Structurally Unprecedented Bioactive Novel-Type Alkaloid from a Sponge-Derived Fungus. In *Sponges (Porifera)*; Müller, W. E. G., Ed.; Springer Verlag: Berlin, 2003; pp 231−253.

(9) Bringmann, G.; Lang, G.; Gulder, T. A. M.; Tsuruta, H.; Mühlbacher, J.; Maksimenka, K.; Steffens, S.; Schaumann, K.; Stöhr, R.; Wiese, J.; Imhoff, J. F.; Perovic-Ottstadt, S.; Boreiko, O.; Müller, W. E. G. *Tetrahedron* **2005**, *61*, 7252.

(10) Throughout this manuscript, we are using the terms endo and exo to describe the orientation of the C7 alkyl group relative to the cis-fused bicyclic ring.

(11) Volp, K. A.; Johnson, D. M.; Harned, A. M. *Org. Lett.* **2011**, *13*, 4486.

(12) Reference 4, pp 191−211.

(13) For examples of γ-butyrolactones fused to a saturated six-membered ring, see: (a) Smith, A. B., III; Richmond, R. E. *J. Am. Chem. Soc.* **1983**, *105*, 575. (b) Taschner, M. J.; Shahripour, A. *J. Am. Chem. Soc.* **1985**, *107*, 5570. (c) Carda, M.; Marco, J. A. *Tetrahedron* **1992**, *48*, 9789. (d) Bermejo, F. A.; Rico-Ferreira, R.; Bamidele-Sanni, S.; García-Granda, S. *J. Org. Chem.* **2001**, *66*, 8287. (e) Maulide, N.; Markó, I. E. *Chem. Commun.* **2006**, 1200.

(14) For examples of γ-butyrolactones fused to an unsaturated six-membered ring, see: (a) Davis, K. M.; Carpenter, B. K. *J. Org. Chem.* **1996**, *61*, 4617. (b) Liu, C.; Bao, G.; Burnell, D. J. *J. Chem. Soc., Perkin Trans. 1* **2001**, 2644. (c) Jung, M. E.; Im, G.-Y. J. *J. Org. Chem.* **2009**, *74*, 8739.

(15) For examples in which a second alkyl group is added to a bicyclic γ-butyrolactone, see: (a) Welch, S. C.; Prakasa Rao, A. S. C.; Gibbs, C. G.; Wong, R. Y. *J. Org. Chem.* **1980**, *45*, 4077. (b) Ishihara, J.; Nonaka, R.; Terasawa, Y.; Tadano, K.-i.; Ogawa, S. *Tetrahedron: Asymmetry* **1994**, *5*, 2217. (c) Molander, G. A.; Harris, C. R. *J. Am. Chem. Soc.* **1995**, *117*, 3705.

(16) Tello-Aburto, R.; Kalstabakken, K. A.; Volp, K. A.; Harned, A. M. *Org. Biomol. Chem.* **2011**, *9*, 7849.

(17) *CRC Handbook of Chemistry and Physics*, 93rd ed., CRC: Boca Raton, FL; pp 15-13−15-22.

(18) We have made several attempts at utilizing a retro-Michael process to epimerize the C7 stereocenter. Unfortunately, all efforts have resulted in either no change of d.r. or decarboxylation of the *t*-butyl ester after elevated temperatures and prolonged reaction times.

(19) Diastereomers were identified as endo or exo based on the chemical shifts and splitting patterns of the C6 methyne proton compared to the known diastereomers of **3** and **5** as well as observed NOE enhancements (see the Supporting Information for details).

(20) Zhao, Y.; Truhlar, D. G. *Theor. Chem. Acc.* **2008**, *120*, 215.

(21) (a) Becke, A. D. *J. Chem. Phys.* **1993**, *98*, 5648. (b) Lee, C.; Yang, W.; Parr, R. G. *Phys. Rev. B* **1988**, *37*, 785.

(22) Hehre, W. J.; Radom, L.; Schleyer, P. v. R.; Pople, J. A. *Ab Initio Molecular Orbital Theory*; Wiley: New York, 1986.

(23) When MeCl was used to alkylate malonate **6** (Cs$_2$CO$_3$, MeCN, rt, 24 h), the alkylation product **5** was formed (61% yield, 64% conversion) with a 5.4:1 d.r. (endo:exo) as measured by HPLC. See the Experimental Section for details.

(24) Zhao, Y.; Truhlar, D. G. *Acc. Chem. Res.* **2008**, *41*, 157.

(25) Johnson, E. R.; Mackie, I. D.; DiLabio, G. A. *J. Phys. Org. Chem.* **2009**, *22*, 1127.

(26) Steinmann, S. N.; Wodrich, M. D.; Corminboeuf, C. *Theor. Chem. Acc.* **2010**, *127*, 429.

(27) Zhao, Y.; Truhlar, D. G. *Chem. Phys. Lett.* **2011**, *502*, 1.

(28) Wheeler, S. E.; Houk, K. N. *J. Am. Chem. Soc.* **2008**, *130*, 10854.

(29) Wheeler, S. E.; McNeil, A. J.; Müller, P.; Swager, T. M.; Houk, K. N. *J. Am. Chem. Soc.* **2010**, *132*, 3304.

(30) Zheng, J.; Zhao, Y.; Truhlar, D. G. *J. Chem. Theory Comput.* **2009**, *5*, 808.

(31) Tang, S.-Y.; Shi, J.; Guo, Q.-X. *Org. Biomol. Chem.* **2012**, *10*, 2673.

(32) Including Cs in these calculations would require expanded basis sets, which would make the calculations more involved. However, the experimental results using K$_2$CO$_3$ and Cs$_2$CO$_3$ are quite similar (Table 2), indicating that models including K should be a reasonable approximation for experiments with Cs.

(33) We are using the syn and anti descriptors to define the relative orientation of the carbonyl oxygen atoms.

(34) The endo and exo transition states leading from **16A$_1$** and **16A$_2$** (M = Na and K) were calculated using B3LYP. In all cases, these transition states were higher in energy than those leading from **16S** (for M = Na: $\Delta G^{\ddagger}_{syn} - \Delta G^{\ddagger}_{anti} = -5.0$ to -15.0 kcal; for M = K: $\Delta G^{\ddagger}_{syn} - \Delta G^{\ddagger}_{anti} = -4.4$ to -11.1 kcal). Other than the orientation of the exocyclic ester and counterion, there were no major structural deviations in these transition states.

(35) (a) Caramella, P.; Rondan, N. G.; Padden-Row, M. N.; Houk, K. N. *J. Am. Chem. Soc.* **1981**, *103*, 2438. (b) Rondan, N. G.; Paddon-Row, M. N.; Caramella, P.; Mareda, J.; Mueller, P. H.; Houk, K. N. *J. Am. Chem. Soc.* **1982**, *104*, 4974. (c) Paddon-Row, M. N.; Rondan, N. G.; Houk, K. N. *J. Am. Chem. Soc.* **1982**, *104*, 7162. (d) Houk, K. N.; Paddon-Row, M. N.; Rondan, N. G.; Wu, Y.-D.; Brown, F. K.; Spellmeyer, D. C.; Metz, J. T.; Li, Y.; Loncharich, R. J. *Science* **1986**, *231*, 1108.

(36) The Houk model is based on previous observations made by Felkin, Seebach, Fukui, and Anh. See: (a) Cherest, M.; Felkin, H.; Prudent, N. *Tetrahedron Lett.* **1968**, 2199. (b) Cherest, M.; Felkin, H. *Tetrahedron Lett.* **1968**, 2205. (c) Seebach, D.; Maetzke, T.; Petter, W.; Klötzer, B.; Plattner, D. A. *J. Am. Chem. Soc.* **1991**, *113*, 1781. (d) Inagaki, S.; Fukui, K. *Chem. Lett.* **1974**, 509. (e) Anh, N. T.; Eisenstein, O.; Lefour, J.-M.; Dau, M.-E. T. H. *J. Am. Chem. Soc.* **1973**, *95*, 6146.

(37) Martinelli, M. J.; Peterson, B. C.; Khau, V. V.; Hutschison, D. R.; Leanna, M. R.; Audia, J. E.; Droste, J. J.; Wu, Y.-D.; Houk, K. N. *J. Org. Chem.* **1994**, *59*, 2204.

(38) Lucero, M. J.; Houk, K. N. *J. Org. Chem.* **1998**, *63*, 6973.

(39) Cheong, P. H.-Y.; Yun, H.; Danishefsky, S. J.; Houk, K. N. *Org. Lett.* **2006**, *8*, 1513.

(40) Wang, H.; Kohler, P.; Overman, L. E.; Houk, K. N. *J. Am. Chem. Soc.* **2012**, *134*, 16054.

(41) Bur, S. K.; Martin, S. F. *Org. Lett.* **2000**, *2*, 3445.

(42) Carreño, M. C.; García-Cerrada, S.; Urbano, A.; Di Vitta, C. *J. Org. Chem.* **2000**, *65*, 4355.

(43) Tredwell, M.; Luft, J. A. R.; Schuler, M.; Tenza, K.; Houk, K. N.; Gouverneur, V. *Angew. Chem., Int. Ed.* **2008**, *47*, 357.

(44) Lucero, M. J.; Houk, K. N. *J. Am. Chem. Soc.* **1997**, *119*, 826.

(45) Ando, K.; Green, N. S.; Li, Y.; Houk, K. N. *J. Am. Chem. Soc.* **1999**, *121*, 5334.

(46) Meyers, A. I.; Seefeld, M. A.; Lefker, B. A. *J. Org. Chem.* **1996**, *61*, 5712 and references therein.

(47) Calculations reported by Meyers and co-workers postulated that electronic factors were responsible for the diastereoselectivity. See: (a) Meyers, A. I.; Seefeld, M. A.; Lefker, B. A.; Blake, J. F. *J. Am. Chem. Soc.* **1997**, *119*, 4565. (b) Meyers, A. I.; Seefeld, M. A.; Lefker, B. A.; Blake, J. F.; Williard, P. G. *J. Am. Chem. Soc.* **1998**, *120*, 7429 . This was refuted by the work reported in ref 45.

(48) Meyers was able to rule out a Cieplak-type effect ((a) Cieplak, A. S. *J. Am. Chem. Soc.* **1981**, *103*, 4540.) as the controlling influence. See: (b) Meyers, A. I.; Wallace, R. H. *J. Org. Chem.* **1989**, *54*, 2509.

(49) van der Waals radii: (H: 1.20 Å, C: 1.70 Å, O: 1.52 Å). See: Bondi, A. *J. Phys. Chem.* **1964**, *68*, 441.

(50) (a) Maria, P.-C.; Gal, J.-F. *J. Phys. Chem.* **1985**, *89*, 1296. (b) Gal, J.-F.; Maria, P.-C.; Massi, L.; Mayeux, C.; Burk, P.; Tammiku-Taul, J. *Int. J. Mass Spectrom.* **2007**, *267*, 7. (c) Laurence, C.; Gal, J.-F. *Lewis Basicity and Affintiy Scale. Data and Measurement*; Wiley: West Sussex, U.K., 2010; pp 323−399.

(51) Marenich, A. V.; Cramer, C. J.; Truhlar, D. G. *J. Phys. Chem. B* **2009**, *113*, 6378.

(52) For a discussion on strengths and limitations associated with solvent models, see: Cramer, C. J. *Essentials of Computational*

Chemistry: Theories and Models, 2nd ed.; Wiley: West Sussex, U.K., 2004; pp 385−427.

(53) Wang, H.; Michalak, K.; Michalak, M.; Jinénez-Osés, G.; Wicha, J.; Houk, K. N. *J. Org. Chem.* **2010**, *75*, 762.

(54) The alkylation of a thioether-containing malonate derived from enone **6** was also attempted. Unfortunately, this reaction was complicated by the production of a significant amount of *endo*-**5**, *exo*-**5**, and **6**. See the Supporting Information (Scheme S1) for more details.

(55) Frisch, M. J.; Trucks, G. W.; Schlegel, H. B.; Scuseria, G. E.; Robb, M. A.; Cheeseman, J. R.; Scalmani, G.; Barone, V.; Mennucci, B.; Petersson, G. A.; Nakatsuji, H.; Caricato, M.; Li, X.; Hratchian, H. P.; Izmaylov, A. F.; Bloino, J.; Zheng, G.; Sonnenberg, J. L.; Hada, M.; Ehara, M.; Toyota, K.; Fukuda, R.; Hasegawa, J.; Ishida, M.; Nakajima, T.; Honda, Y.; Kitao, O.; Nakai, H.; Vreven, T.; Montgomery, J. A., Jr.; Peralta, J. E.; Ogliaro, F.; Bearpark, M.; Heyd, J. J.; Brothers, E.; Kudin, K. N.; Staroverov, V. N.; Keith, T.; Kobayashi, R.; Normand, J.; Raghavachari, K.; Rendell, A.; Burant, J. C.; Iyengar, S. S.; Tomasi, J.; Cossi, M.; Rega, N.; Millam, J. M.; Klene, M.; Knox, J. E.; Cross, J. B.; Bakken, V.; Adamo, C.; Jaramillo, J.; Gomperts, R.; Stratmann, R. E.; Yazyev, O.; Austin, A. J.; Cammi, R.; Pomelli, C.; Ochterski, J. W.; Martin, R. L.; Morokuma, K.; Zakrzewski, V. G.; Voth, G. A.; Salvador, P.; Dannenberg, J. J.; Dapprich, S.; Daniels, A. D.; Farkas, O.; Foresman, J. B.; Ortiz, J. V.; Cioslowski, J.; Fox, D. J. *Gaussian 09*; Gaussian, Inc.: Wallingford, CT, 2010.

(56) Wheeler, S. E.; Houk, K. N. *J. Chem. Theory Comput.* **2010**, *6*, 395.